Numerical Modelling and Optimization of 3D Surface Roughness Forecasting in Milling

Juanjuan Zhao, Yanzhi Guan, and Zhen Chen

Abstract—**The quality of micro-milling parts is greatly influenced by surface roughness. However, the evaluation of surface roughness solely based on two-dimensional (2D) parameters is limited. In order to more comprehensively reflect the processing quality and surface performance in the micro-milling process, this paper selected three representative parameters, namely S_a, S_q, and S_{dr}, as the characterization parameters for three-dimensional surface roughness (3D-SR). The mapping relationship between the 3D-SR and spindle rotational velocity, feed velocity, radial machining depth, axial machining depth was experimentally investigated, then the relationship models were established using response surface method (RSM). Subsequently, this study employed the backpropagation neural network (BPNN) to predict the 3D-SR. While maintaining the same BPNN topology, we introduced particle swarm optimization (PSO) as well as genetic algorithm (GA) to enhance the initial thresholds and connection weights of the network. This allowed us to establish three prediction models for 3D-SR. The results indicate that the PSO-BPNN prediction models have better prediction performance than other models of this paper.**

Index Terms—**milling, 3D-SR forecasting, response surface method, neural network optimization**

I. Introduction

Milling is a common machining technology in the manufacturing industry, which has the ability to produce complex geometric shapes. The machining accuracy and quality of a workpiece are directly influenced by the milling process parameters, making them crucial to the overall product quality [1]. The interaction between the cutting tool and the work material during the milling operation directly impacts the surface morphology of the work material, which in turn affects the resulting surface roughness [2]. Therefore, the control of milling process parameters is of great importance to enhance tool life and product quality.

The research on milling processing mostly adopts the experimental method, which is accurate but time-consuming and labor-intensive [3]. Consequently, the forecast of roughness has attracted the attention of scholars. Prabhakar [4] developed an integrated approach using Fast Fourier to predict surface roughness for milled surfaces. Zhang [5] proposed a method using a least squares support vector machine to predict R_a of machined surfaces and demonstrated the algorithm's feasibility. Kong [6] achieved effective prediction of R_a in milling process by employing Bayesian linear regression method. Scholars' research on surface roughness of milling mainly focuses on two-dimensional (2D) surface roughness. Obtained from the contour trajectory, 2D surface roughness cannot reflect the surface topography of the geometric information. Three-dimensional (3D) surface roughness is obtained from the surface and has ability to characterize the contour and characteristics of the workpiece surface more comprehensively [7]. Molnár [8] determined the minimum evaluation areas of a few frequently used 3D height parameters which contributed to saving measurement time and enabling large scale production. Jayabarathi [9] established a relationship between characteristic features and 3D-SR. Hoła [10] conducted a study to assess the usefulness of 3D-SR in nondestructive evaluation for pull-off adhesion in concrete layers.

Currently, most scholars focus on the prediction of 2D surface roughness, with limited research dedicated to the prediction of 3D-SR. We aim to address this research gap in this study. The organization for this study is as outlined below: Three representative 3D-SR parameters, namely S_a, S_q, and S_{dr}, were selected as the research objects. Then, the influence of machining parameters on 3D-SR was analyzed based on response surface method (RSM). Subsequently, the 3D-SR forecasting models based on BPNN were established. Then we employed genetic algorithm as well as particle swarm optimization improve the BPNN model. By doing so, we aimed to enhance the performance and reliability of the prediction models. Finally, we conducted a comparative analysis to assess the performance of different models and evaluated the precision of the prediction models.

II. Materials and Methods

A. Experimental scheme

7075 aluminum alloy, known for its high strength and corrosion resistance, finds extensive applications in various industries including aerospace, ships, automobiles, etc. In this study, 7075 alloy was milled with the tool of 1 mm in diameter. The experiment was designed using the Box-Behnken Design. The machining parameters considered were spindle rotational velocity (n), feed velocity (v_f), radial cutting depth (a_e), as well as axial cutting depth (a_p). Three levels were selected for each parameter according to the machining experience. The scheme is shown in Table 1.

Manuscript received December 18, 2022; revised July 30, 2023. This work was substantially supported by the Natural Science Basic Research Program of Shaanxi (Program No. 2022JQ-503), Doctoral Research Startup Fund of Xi'an Aeronautical Institute(2021KY0216).

Juanjuan Zhao is an associate professor at Mechanical Engineering Department, Shanxi Engineering Vocational College, Taiyuan Shanxi 030009, China (zhaojuanjuan_8@163.com).

Yanzhi Guan is an associate professor at School of Mechanical and Material Engineering, North China University of Technology, Beijing 100144, China (gyz@ncut.edu.cn).

Zhen Chen is a lecturer at School of Mechanical Engineering, Xi'an Aeronautical University, Xi'an Shaanxi 710077, China (chenzhen@xaau.edu.cn).

B. Data processing

This paper selected three representative 3D-SR parameters for prediction in the parameters of ISO-25178-2, including S_a, S_q and S_{dr}. In the scale-limited surface, arithmetical mean height (S_a) indicates how much the contour deviates from reference surface. Root mean square height (S_q) shows standard deviation of surface height distribution. The developed interfacial area ratio (S_{dr}) measures overall performance of surface and can distinguish between surfaces with similar amplitudes and average roughness. To obtain 3D-SR, we used a confocal sensor to scan the measuring area of the workpiece surface, and the resulting data is presented in Table 1. To avoid the fitting error caused by the difference in the data range and the dimensional unit, it is necessary to standardize the data as shown in formula (1):

$$x = \left(X - X_{\min}\right) / \left(X_{\max} - X_{\min}\right) \quad (1)$$

where x is data before normalization, X is data after normalization; $X_{\min}$ is minimum value in X, $X_{\max}$ is maximum values in X.

TABLE I
EXPERIMENTAL PARAMETER SCHEDULE AND MEASUREMENT RESULTS

No.	n (r/min)	v_f (mm/min)	a_p (μm)	a_e (mm)	S_a	S_q	S_{dr}
1	8000	100	40	0.1	0.161	0.207	0.030
2	8000	300	60	0.2	0.211	0.271	0.033
3	6000	200	40	0.1	0.164	0.212	0.031
4	10000	200	20	0.2	0.145	0.189	0.027
5	6000	200	60	0.2	0.199	0.256	0.040
6	8000	200	60	0.1	0.142	0.188	0.018
7	8000	200	40	0.2	0.137	0.178	0.026
8	8000	200	20	0.1	0.166	0.211	0.031
9	8000	200	40	0.2	0.152	0.198	0.030
10	8000	100	40	0.3	0.153	0.199	0.027
11	10000	200	40	0.1	0.151	0.200	0.028
12	8000	200	40	0.2	0.141	0.184	0.028
13	10000	100	40	0.2	0.147	0.190	0.025
14	8000	200	20	0.3	0.201	0.261	0.033
15	6000	100	40	0.2	0.135	0.177	0.026
16	10000	200	60	0.2	0.180	0.242	0.042
17	10000	300	40	0.2	0.180	0.232	0.030
18	8000	100	20	0.2	0.130	0.168	0.024
19	8000	200	40	0.2	0.159	0.218	0.032
20	6000	200	20	0.2	0.159	0.206	0.035
21	8000	200	60	0.3	0.192	0.250	0.033
22	8000	200	40	0.2	0.145	0.191	0.030
23	6000	300	40	0.2	0.233	0.302	0.052
24	8000	100	60	0.2	0.141	0.184	0.027
25	8000	300	20	0.2	0.168	0.222	0.032
26	6000	200	40	0.3	0.223	0.290	0.038
27	8000	300	40	0.1	0.157	0.202	0.030
28	10000	200	40	0.3	0.143	0.183	0.027
29	8000	300	40	0.3	0.234	0.302	0.042

III. ESTABLISHMENT OF 3D-SR PREDICTION MODELS

A. 3D-SR prediction model based on the BPNN

BPNN is a typical multi-layer feedforward network, which consists of an input layer, a hidden layer, as well as an output layer. According to error of the output, connection weight and the threshold value of each layer are continuously adjusted and corrected through training [11]. In general, the prediction results of multi-layer networks in large sample space are more precise than that of one-layer networks, but the required time is greatly increased. In this study, a three-layer BP n topology with 3D-SR parameters was established for a small sample space, as shown in Fig. 1. Out of the 29 experimental data points, 5 were repeated experiments. To account for this, we took the average value of these 5 results and used it as the result for the 7th experiment. We then moved the serial numbers of the remaining experiments forward successively, resulting in a total of 25 unique experiments. The first 17 experiments were taken to train the network, and the remaining 8 experiments were predicted. The input layer of the network consists of four nodes, namely spindle rotational velocity, feed velocity, radial machining depth, as well as axial machining depth. And the number of nodes in hidden layer is twice that in input layer, plus one. The output node is the 3D-SR parameter. The main parameters of prediction model are displayed in Table 2.

B. 3D-SR prediction model based on GA-BPNN and PSO-BPNN

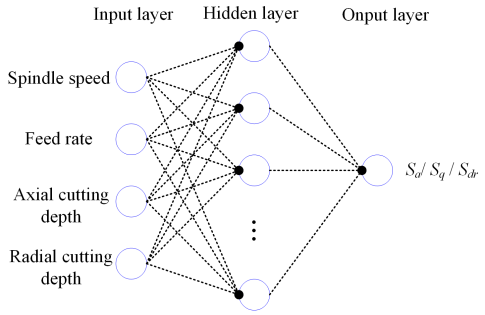

Fig. 1. BP neural network topology

TABLE II
MAIN PARAMETERS OF THE BPNN PREDICTION MODEL

Input layer nodes	Hidden layer nodes	Output layer node	Learning velocity	Maximum number of training	Training requirements precision
4	9	1	0.1	10000	0.00001

The original thresholds and weights of BPNN generally adopt system default values or are determined based on experience, which can significantly impact the model and may reduce the prediction precision and convergence rate [12]. Thus, we introduced GA as well as PSO to optimize the original thresholds and weights of BPNN.

GA simulates the evolutionary rules of nature. Its basic idea is "survival of the fittest" and "natural selection". There are three operational operations of selection, crossover, and mutation, thus leaving excellent varieties and eliminating inferior varieties [13]. The search mechanism belongs to the parallel search. Compared with serial search mechanism of the neural network [14] ~ [16], GA-BPNN has a good global search ability to prevent falling into local minimum values. In BPNN optimized by GA, the connection thresholds and

weights of neural networks are encoded as populations. The MSE that between estimated output and forecasted output is used as a fitness function. Through a process of chromosome selection, crossover, and mutation, fitness function is applied to judge the fitness in the populations and optimize the connection weights and thresholds of neural network.

PSO is a variety of random search algorithm which based on group collaboration in bird groups. Both PSO and GA belong to parallel search mechanism, which can be used for global optimization. The GA shares information between the chromosomes and the entire population moves towards the optimal region. PSO relies on information sharing between individuals to constantly move to find the global optimal solution. In contrast to GA, PSO preserves the optimal solution from the previous iteration and compares it with the optimal solution from the current iteration to achieve stepwise optimization. It is easier to implement and has faster convergence than GA. In this paper, we used the PSO algorithm is used to improve the origin thresholds and weights of BPNN and established PSO-BPNN prediction model.

IV. Discussion

A. Parameter Influencing Analysis

The mapping relationship between design parameters and target response is obtained through regression analysis by RSM, which is typically represented by a second-order regression model. We obtained the mapping relationship between RSM-based processing parameters and 3D-SR as follows:

$$\begin{aligned} S_a = {} & 0.30468 - 2.25\times10^{-5}\cdot n - 1.41\times10^{-4}\cdot v_f \\ & - 2.38792\times10^{-3}\cdot a_p - 0.29925\cdot a_e - 8.05\times10^{-8}\cdot n\cdot v_f \\ & - 3.6875\times10^{-8}\cdot n\cdot a_p - 8.4125\times10^{-5}\cdot n\cdot a_e \\ & + 4.0625\times10^{-6}\cdot v_f\cdot a_p + 2.1275\times10^{-3}\cdot v_f\cdot a_e \\ & + 1.9375\times10^{-3}\cdot a_p\cdot a_e + 3.12396\times10^{-9}\cdot n^2 \\ & + 1.15208\times10^{-6}\cdot v_f^2 \quad 2.35208\times10^{-5}\cdot a_p^2 + 1.59833\ a_e^2 \end{aligned} \tag{2}$$

$$\begin{aligned} S_q = {} & 0.34738 - 2.61358\times10^{-5}\cdot n - 3.72333\times10^{-5}\cdot v_f \\ & - 3.00367\times10^{-3}\cdot a_p - 0.17815\cdot a_e - 1.03875\times10^{-7}\cdot n\cdot v_f \\ & + 1.8125\times10^{-8}\cdot n\cdot a_p - 1.19125\times10^{-4}\cdot n\cdot a_e \\ & + 4.15\times10^{-6}\cdot v_f\cdot a_p + 2.7125\times10^{-3}\cdot v_f\cdot a_e \\ & + 1.5375\times10^{-3}\cdot a_p\cdot a_e + 3.83583\times10^{-9}\cdot n^2 \\ & + 1.24558\times10^{-6}\cdot v_f^2 + 2.84521\times10^{-5}\cdot a_p^2 + 1.87183\ a_e^2 \end{aligned} \tag{3}$$

$$\begin{aligned} S_{dr} = {} & 0.08106 - 1.23275\times10^{-5}\cdot n + 1.59017\times10^{-4}\cdot v_f \\ & - 8.09083\times10^{-4}\cdot a_p - 0.03965\cdot a_e - 2.6125\times10^{-8}\cdot n\cdot v_f \\ & + 5.75\times10^{-8}\cdot n\cdot a_p - 8.75\times10^{-6}\cdot n\cdot a_e - 3.5\times10^{-7}\cdot v_f\cdot a_p \\ & + 3.9\times10^{-4}\cdot v_f\cdot a_e + 1.5875\times10^{-3}\cdot a_p\cdot a_e \\ & + 9.49375\times10^{-10}\cdot n^2 + 9.475\times10^{-8}\cdot v_f^2 \\ & + 1.80625\times10^{-6}\cdot a_p^2 - 0.01275\cdot a_e^2 \end{aligned} \tag{4}$$

The variance of the 3D-SR regression models based on RSM was analyzed to test the fitting accuracy of the models. The *p*-value indicates reliability. The *p*-values of S_a, S_q, S_{dr} are 0.0006, 0.0009, 0.0306, respectively, all of which are less than 0.05, In contrast, the *p*-values of the lack of fit are all greater than 0.05, that is, the three models are significant and the lack of fit terms are not significant, indicating that regression models are well fitted and reliable.

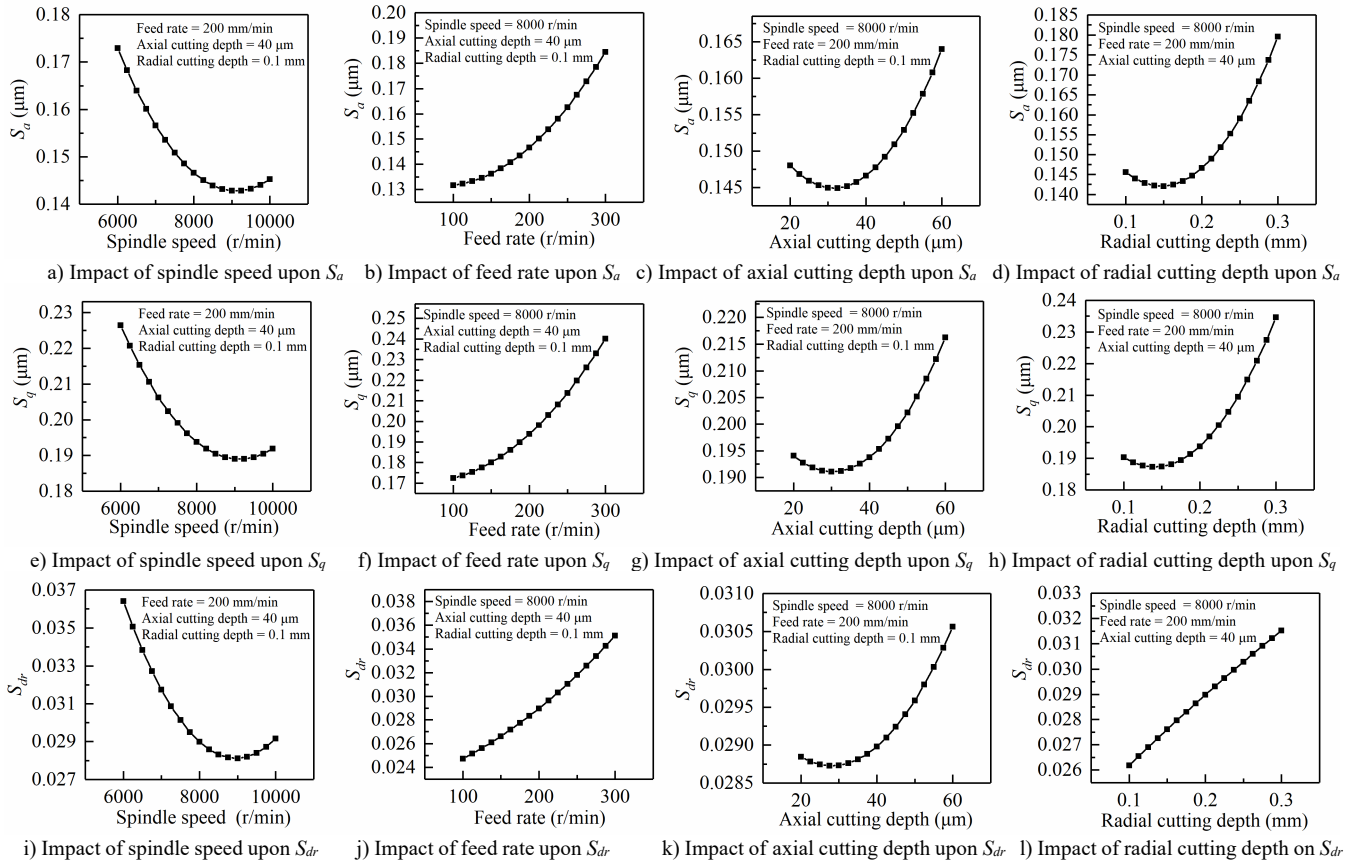

a) Impact of spindle speed upon S_a b) Impact of feed rate upon S_a c) Impact of axial cutting depth upon S_a d) Impact of radial cutting depth upon S_a

e) Impact of spindle speed upon S_q f) Impact of feed rate upon S_q g) Impact of axial cutting depth upon S_q h) Impact of radial cutting depth upon S_q

i) Impact of spindle speed upon S_{dr} j) Impact of feed rate upon S_{dr} k) Impact of axial cutting depth upon S_{dr} l) Impact of radial cutting depth on S_{dr}

Fig. 2. Influence of main process parameters upon 3D surface roughness parameters.

To investigate the impact of various process parameters on 3D-SR during micro-milling and understand the variation of 3D-SR within the processing parameters studied, this section presents the relationship between process parameters and 3D-SR based on the RSM models, which is illustrated in Fig. 2.

Figure 2(a), 2(e), and 2(i) indicate that when radial cutting depth, the feed rate, as well as axial cutting depth are constant, S_a, S_q and S_{dr} exhibit similar variation trends. As spindle speed rises, the residual height and the feed per tooth decrease, while the tool chatter will be intensified. All three parameters gradually decrease and then increase, reaching a minimum value around a spindle speed of 9000 r/ min. Similarly, in Fig. 2(b), 2(f), and 2(j), when spindle rotational velocity, radial machining depth as well as axial machining depth, are constant, an increase in feed rate results in increased feed per tooth and surface residual height, with S_a, S_q and S_{dr} gradually increasing. According to Fig. 2(c), 2(g), and 2(k), the trends of S_a, S_q and S_{dr} are similar. If the cutting thickness falls below the minimum cutting threshold, size effect will occur, resulting in failure to control surface quality. S_a, S_q and S_{dr} gradually decrease and then increase as axial cutting depth a_p rises, reaching a minimum point near the axial cutting depth of 30μm. Finally, according to Fig. 2(d), 2(h), and 2(l), when feed rate, the spindle speed, as well as axial cutting depth, are held constant, increasing the radial cutting depth initially leads to a decrease in S_a and S_q. However, they eventually reach a minimum value around a radial cutting depth of 0.05 mm before increasing again. In contrast, S_{dr} increases almost linearly with increasing radial cutting depth.

B. Prediction accuracy result

Fig. 3 presents the forecast and experimental results for the three forecasting models in this paper. It demonstrates that predicted output values of the three neural network models closely match the actual values, indicating that they are capable of accurately predicting S_a, S_q and S_{dr}.

To assess the accuracy of the models, we selected three performance indicators including MAE, MSE, and MAPE, as shown in Table 3. MAE avoids the mutual offset of errors, thus reflecting the actual level of error. MSE can evaluate the degree of change of data. MAPE describes the accuracy of the model. For these three roughness parameters, the values of the three performance indicators in the prediction models based on BPNN are less than those of the forecasting models which based on the GA-BPNN as well as PSO-BPNN, indicating that optimizing the origin thresholds and weights of the neural network can result in better accuracy.

$$MAE = \frac{1}{N}\sum_{i=1}^{N}|Y_i - O_i| \tag{5}$$

$$MSE = \frac{1}{N}\sum_{i=1}^{N}(Y_i - O_i)^2 \tag{6}$$

$$MAPE = \frac{1}{N}\sum_{i=1}^{N}\left|\frac{Y_i - O_i}{Y_i}\right| \times 100\% \tag{7}$$

where Y_i is measurement value for the i-th experiment, O_i is prediction value for the i-th experiment.

After conducting extensive experiments, it was discovered that not all models achieved the desired accuracy. When using BPNN prediction models, the origin thresholds and connection weights of the network are randomly generated,

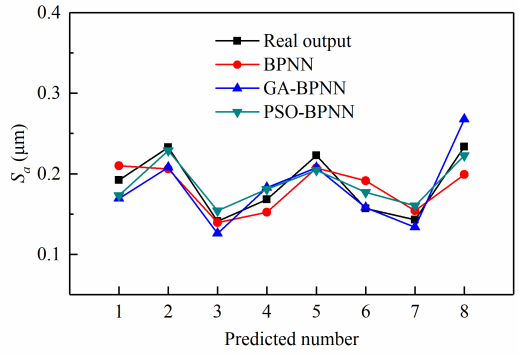

a) Results for S_a

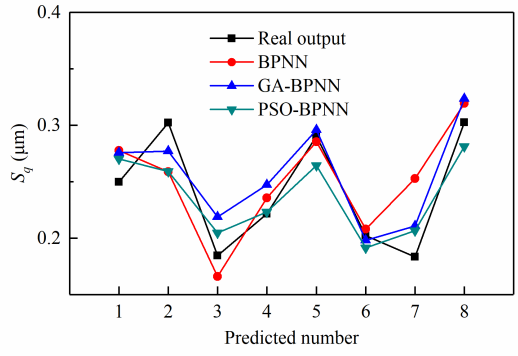

b) Results for S_q

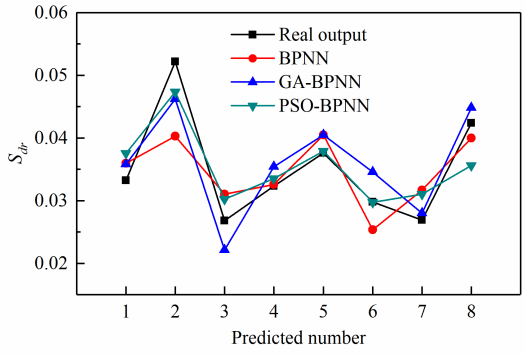

c) Results for S_{dr}

Fig. 3. Iteration speed of BPNN prediction models.

TABLE III
MAIN PARAMETERS OF THE BPNN PREDICTION MODEL

Parameters	Models	MAE	MSE	MAPE
S_a	BPNN	0.0197	0.0005	0.1033
	GA--BPNN	0.0170	0.0004	0.0878
	PSO-BPNN	0.0145	0.0002	0.0832
S_q	BPNN	0.0251	0.0010	0.1124
	GA--BPNN	0.0212	0.0006	0.0936
	PSO-BPNN	0.0208	0.0006	0.0850
S_{dr}	BPNN	0.0042	2.8079×10^{-5}	0.1173
	GA--BPNN	0.0034	1.4043×10^{-5}	0.0997
	PSO-BPNN	0.0031	1.4888×10^{-5}	0.0891

which can significantly impact the results. During the training process, the fitness value may stick in a small-scale minimum, leading to reduced accuracy. Both the GA-PSO and PSO-BPNN prediction models refine the origin thresholds and connection weights for the network, resulting in good prediction results with little difference in accuracy.

However, in the optimization process of the origin thresholds and connection weights for the network, although genetic operation for GA can reduce possibility of falling into a minimum value, it may also lead to deviation from the optimal solution, thereby increasing training time. Similar to GA, the PSO algorithm is also susceptible to becoming trapped in a local minimum. In the next section, we will explore the speed of model iteration.

C. Model convergence analysis

The iteration speed of GA-BPNN and PSO-BPNN is shown in Fig.4, which illustratess that PSO algorithm generally achieves better convergence than GA. As a matter of fact, GA tends to converge before reaching a given precision or needs more time to find the optimal solution. In comparison, PSO is easier or faster to find the optimal solution than GA.

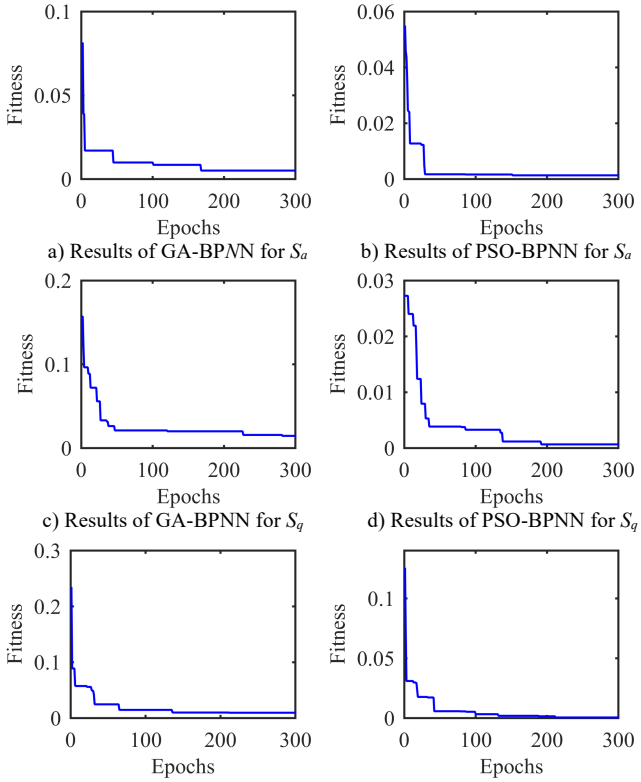

a) Results of GA-BP*N*N for S_a b) Results of PSO-BPNN for S_a

c) Results of GA-BPNN for S_q d) Results of PSO-BPNN for S_q

e) Results of GA-BPNN for S_{dr} f) Results of PSO-BPNN for S_{dr}

Fig. 4. Comparison of iteration speed between GA and PSO.

V. Conclusions

The objective in this paper is to explore the correlation between the 3D-SR parameters and four machining parameters, namely spindle rotational velocity, feed velocity, radial machining depth, as well as axial machining depth, utilizing RSM method. In view of the current rare 3D-SR prediction problem, this paper applied BPNN theory to the prediction of milling 3D-SR, and set up four milling 3D-SR prediction models. The effectiveness of the forecasting model was assessed by calculating the corresponding performance parameters and comparing the iterative convergence. This paper draws the following main conclusions through experiments and theoretical analysis:

(1) This study investigated the impact of micro-milling parameters on 3D-SR by establishing relationship models between 3D-SR parameters and machining parameters using the RSM method. The influence of various processing parameters on 3D-SR was analyzed based on these models.

(2) S_a, S_q and S_{dr} of milling were predicted by BPNN, GA and PSO were introduced to fine-tune the origin thresholds and connection weights for BPNN respectively, which improves accuracy as well as optimization speed for the model.

(3) Among all the prediction models of three 3D-SR parameters, the 3D-SR prediction models based on PSO-BPNN achieve optimal performance and a certain level of robustness, exhibiting the most satisfactory results comprehensively.

References

[1] J. Yan, L. Li, "Multi-objective optimization of milling parameters–the trade-offs between energy, production rate and cutting quality," Journal of Cleaner Production, vol. 52, no.1, pp462-471, 2013.

[2] F. Ozturk, S. Toros, S. Kilic, "Tensile and spring-back behavior of DP600 advanced high strength steel at warm temperatures," Journal of Iron and Steel Research International, vol. 16, no.6, pp41-46, 2009.

[3] K. Danesh Narooei, R. Ramli, "Optimal Selection of Cutting Parameters for Surface Roughness in Milling Machining of AA6061-T6," International Journal of Engineering, vol. 35, no.6, pp1170-1177, 2022.

[4] D. V. N. Prabhakar, M. S. Kumar, A. G. Krishna, "A Novel Hybrid Transform approach with integration of Fast Fourier, Discrete Wavelet and Discrete Shearlet Transforms for prediction of surface roughness on machined surfaces," Measurement, vol.164, no.1, pp108011, 2020.

[5] N. Zhang, D. Shetty, "An effective LS-SVM-based approach for surface roughness prediction in machined surfaces," Neurocomputing, vol. 198, no.1, pp35-39, 2016.

[6] D. Kong, J. Zhu, C. Duan, L. Lu, D. Chen, "Bayesian linear regression for surface roughness prediction," Mechanical Systems and Signal Processing, vol. 142, no.1, pp70-81, 2020.

[7] K. K. Manesh, B. Ramamoorthy, M. Singaperumal, "Numerical generation of anisotropic 3D non-Gaussian engineering surfaces with specified 3D surface roughness parameters," Wear, vol. 268, no. 11, pp 1371-1379, 2010.

[8] V. Molnár, "Minimization Method for 3D Surface Roughness Evaluation Area," Machines, vol. 9, no. 9, pp 92, 2021.

[9] S. B. Jayabarathi, M. M. Ratnam. Correlation Study of 3D Surface Roughness of Milled Surfaces with Laser Speckle Pattern," Sensors, vol. 22, no. 8, pp 42-48, 2022.

[10] J. Hoła, Ł. Sadowski, J. Reiner, S. Stach, "Usefulness of 3D surface roughness parameters for nondestructive evaluation of pull-off adhesion of concrete layers," Construction and Building Materials, vol. 84, no.1, pp111-120, 2015.

[11] D. E. Rumelhart, G. E. Hinton, R. J. Williams, "Learning representations by back-propagating errors," Nature vol. 323, no. 6088, pp 533-536, 1986.

[12] H. Fan, Y. Yan, X. Zhang, X. Cao, J. Ma, "Composite Fault Diagnosis of Rolling Bearing Based on Optimized Wavelet Packet AR Spectrum Energy Entropy Combined with Adaptive No Velocity Term PSO-SOM-BPNN," Journal of Sensors, vol. 11, no. 6, pp 410-421, 2021.

[13] P. He, Y. Fan, B. Pan, Y. Zhu, J. Liu, D. Zhu, "Calibration and verification of dynamic particle flow parameters by the back-propagation neural network based on the genetic algorithm: recycled polyurethane powder," Materials, vol. 12, no. 20, pp 3350, 2019.

[14] J. Liu, Q. Zhang, and Z. Luo, "Dynamical Analysis of Fuzzy Cellular Neural Networks with Periodic Coefficients and Time-varying Delays," IAENG International Journal of Applied Mathematics, vol. 46, no. 3, pp 298-304, 2016.

[15] C. Zhong, Y. Liu, J. Wang, and Z. Li, "LSTM Neural Network Fault Diagnosis Method for Rolling Bearings Based on Information Fusion," IAENG International Journal of Computer Science, vol. 49, no. 4, pp 1088-1098, 2022.

[16] Y. Zhou, X. Ouyang, N. Zhao, H. Xu, and H. Li, "Prescribed Performance Adaptive Neural Network Tracking Control of Strict-Feedback Nonlinear Systems with Nonsymmetric Dead-zone," IAENG International Journal of Applied Mathematics, vol. 51, no. 3, pp 444-452, 2021.